Front. Med. 2025, 19(6): 1252−1268
https://doi.org/10.1007/s11684-025-1164-0

RESEARCH ARTICLE

Azvudine remodels the local immunosuppressive microenvironment and exhibits sustained anti-tumor effects in combination with anti-PD-1 therapies

Limin Jia[1], Zhaoyang Wang[1], Jinfa Du[1], Zhigang Ren[2], Jiandong Jiang (✉)[3], Pan Li (✉)[1]

[1]Drug Discovery Department, Henan Genuine Biotech Limited Inc., Pingdingshan 467002, China; [2]Department of Infectious Diseases, The First Affiliated Hospital of Zhengzhou University, Zhengzhou 450052, China; [3]Institute of Medicinal Biotechnology, Chinese Academy of Medical Science and Peking Union Medical College, Beijing 100050, China

Abstract **The immunosuppressive tumor microenvironment (TME) undermines the efficacy of many cancer therapies. This study investigated the immunomodulatory and anti-tumor activity of Azvudine (FNC), alone or in combination with anti-PD-1 blockade. We established syngeneic tumor models in immunocompetent mice. Single-cell RNA sequencing, flow cytometry, and immunological assays were employed to analyze immune cell reconstitution and functional changes following FNC administration. FNC demonstrated dose- and time-dependent tumor inhibition. It significantly expanded memory T cells, natural killer (NK) cells, and $CD8^+$ cytotoxic T lymphocytes, while reducing the abundance of myeloid-derived suppressor cells (MDSCs). Flow cytometry confirmed these immunological shifts, showing enhanced infiltration of effector immune cells within the TME. Moreover, FNC induced hallmark features of immunogenic cell death (ICD), including the release of damage-associated molecular patterns such as high-mobility group box 1 (HMGB1) and calreticulin. When combined with anti-PD-1 therapy, FNC produced a synergistic anti-tumor effect, leading to durable tumor remission in all treated mice. FNC remodels the TME by mitigating immunosuppression and amplifying anti-tumor immunity, offering a promising strategy to augment existing immunotherapies. Further clinical evaluation is warranted to ascertain the translational potential of FNC in diverse oncologic settings.**

Keywords immunosuppressive microenvironment; Azvudine; myeloid-derived suppressor cells; immunogenic cell death; anti-PD-1 therapy; tumor microenvironment

Introduction

Extensive research indicates that tumors modulate the local immune microenvironment and induce immunosuppressive tumor-infiltrating lymphocytes (TILs) infiltration, creating an immunosuppressive microenvironment. This environment impedes the infiltration and cytotoxic effects of effector immune cells such as cytotoxic T lymphocytes (CTLs) and natural killer (NK) cells. Myeloid-derived suppressive cells (MDSCs) significantly contribute to this process by promoting immunosuppression within the tumor microenvironment (TME). This may be linked to creating an immunosuppressive microenvironment comprising various lymphoid and myeloid cells [1–3]. For instance, MDSCs, in particular, significantly contribute to immunosuppression in the TME [2,4,5]. Their accumulation and infiltration within the TME lead to the inhibition of T and NK cells' proliferation [6].

Tumors can also facilitate immune evasion by expressing the programmed death-ligand 1 (PD-L1) marker, which attenuates the cytotoxic response of activated T cells through programmed death 1 (PD-1) receptor interaction. Therapy employing anti-PD-1 uncovers the tumor by binding to PD-1, thus enhancing tumor recognition by T cells and amplifying the immune response. Although anti-PD-1 therapy has shown clinical efficacy in treatment-naïve solid tumors when used alone or in combination, its effectiveness against heavily treated, resistant, or recurrent tumors remains limited. This lack of efficacy could be substantially attributed to several immunosuppressive mechanisms, such as the

Received December 31, 2024; accepted August 4, 2025
Correspondence: Jiandong Jiang, jiang.jdong@163.com;
Pan Li, panli100@gmail.com

infiltration of MDSCs, which are known for suppressing T cell activity and creating a local immunosuppressive microenvironment. Additionally, tumors often upregulate immune checkpoint molecules like PD-L1, which interact with PD-1 on T cells, further dampening the immune response. Regulatory T cells (Tregs) and other immunosuppressive cells also contribute to the resistance observed with anti-PD-1 therapy. Overcoming these barriers is crucial for improving the outcomes of anti-PD-1 therapies in these challenging cases [7,8]. Therefore, overcoming the core challenge of durable resistance in solid tumors lies in disrupting this immunosuppressive microenvironment.

Azvudine (FNC) is a novel cytidine analog that targets RNA-dependent polymerases, exhibiting both antiviral and anticancer effects. It functions by inhibiting RNA-dependent polymerase enzymes in various viruses and retrotransposons, which reduces cancer genome instability and tumor aggressiveness in liquid tumors [9,10]. FNC also directly impacts liquid tumor cells by inhibiting their adhesion, migration, invasion, and proliferation and induces cell cycle arrest and apoptosis [11]. Simultaneously, FNC has demonstrated potential in enhancing the anti-tumor effects of other drugs. For instance, in *in vitro* studies, the combination of FNC with chemotherapeutic agents such as doxorubicin and methotrexate significantly enhanced cytotoxicity and anti-tumor activity against human lymphoma, lung adenocarcinoma, and acute myeloid leukemia cells through co-delivery mechanisms [9]. Furthermore, in a severe combined immunodeficiency (SCID) mouse xenograft model, FNC, in combination with cisplatin, showed superior tumor growth inhibition in mantle cell lymphoma compared to either agent alone [11].

Based on these findings, we aimed to evaluate the anti-tumor effects of FNC both as monotherapy and in combination with anti-PD-1. The study involved a range of *in vitro* and *in vivo* solid tumor models. Additionally, we will utilize single-cell multi-omics techniques to comprehensively map the regulatory effects of FNC on the dynamics of the TME *in vivo*. Finally, we will assess the *in vivo* anti-tumor efficacy of FNC combined with anti-PD-1 therapy in multiple solid tumors. We hope this study will provide evidence for the anti-tumor effects of FNC and its feasibility in combination with existing anti-tumor therapies.

Experiment details

Cell lines and reagents

Cancer cell lines CT26 and EMT6 were initially obtained from American Type Culture Collection (ATCC) (cat. # CRL-2638 and CRL-2755). H22 was purchased from China Center for Type Culture Collection (CCTCC) (cat. # GDC0091). Anti-PD-1 (anti-mouse PD-1) was purchased from BioXcell (BE0146). The cell culture was performed according to the suppliers' instructions.

In vivo experiments

All experiments were approved by the Institutional Animal Care and Use Committee (IACUC) of WuXi AppTec, CrownBio or Frontage New-Drug, Inc. CT26 cells (0.3×10^6 cells of each mouse) were suspended in 0.1 mL of PBS and injected subcutaneously in the flank of BALB/c or B-NDG for tumor development. Syngeneic models were generated on BALB/c immunocompetent mice strains, and one CT26 model was generated on B-NDG mice strain with immune deficiency. H22 cells (2×10^6 cells of each mouse) were suspended in 0.1 mL of PBS and injected subcutaneously in the flank of BALB/c for tumor development. Treatments were started on days 6−10 after tumor inoculation when the average tumor size reached approximately 50−100 mm^3. 6−10 mice in each group received oral administration once per day of FNC at different dosages. Tumor volumes were measured two or three times per week after randomization in two dimensions using a caliper, and tumor volume was calculated as $V = (\text{length} \times \text{width}^2)/2$. Dosing, tumor, and body weight measurements were conducted in a laminar flow cabinet. To compare tumor volumes of different groups on a pre-specified day, we first used Bartlett's test to check the assumption of homogeneity of variance across all groups. When the *P*-value of Bartlett's test is $\geqslant$ 0.05, we ran one-way ANOVA to test the overall equality of means across all groups. If the *P*-value of the one-way ANOVA is < 0.05, we further performed post hoc testing by running Tukey's HSD (honestly significant difference) tests for all pairwise comparisons and Dunnett's tests for comparing each treatment group with the vehicle group.

Sample preparation and flow cytometry analysis for tils

Tumor samples were washed with cold PBS, followed by fibrous, fat, and necrotic tissue removal. Tumor tissues were minced into small pieces and transferred into Gentle MACS C Tubes prepared with 5 mL of 1 × mixed enzymes. After being treated with program m_imptumor_01_01, samples were digested in the water bath at 37°C for 30 min, followed by another round of m_imptumor_01_01 program treatment. Then, cold PBS (containing 2% FBS) was added to stop the cell from further digestion. Tumor cells were filtered through a 70 μm cell strainer and washed with cold PBS. The corresponding volume of cold PBS was added to resuspend cells according to the number of cell pellets. Cell pellets were further counted and prepared for antibody staining.

Single cells were resuspended with PBS to 1×10^6 cells/100 μL and seeded on a 96-well plate. The plate was centrifuged at 4 °C 450 *g* for 5 min, and the supernatant was discarded. Cells were then resuspended with 100 μL diluted Zombie NIR Live/Dead at 4 °C in the dark for 30 min. After incubation, cells were washed twice with 200 μL cold PBS. Cell pellets were resuspended with 50 μL staining buffer containing Mouse Fc Block (1 μL per well) and incubated at 4 °C in the dark for 5 min. Pacific Orange CD8, BV605 MHCII, BV650 CD25, BV750 CD45, BV785 Ly6C, AF488 CD11c, AF532 CD11b, PE-DZL594 CD49b, APC Ly6G, APC-Cy5.5 CD4, APC-Cy7 CD3, and BV421 CD69 (or isotype) were prepared in 50 μL Brilliant Stain Buffer which then added to cell suspension and incubated at 4 °C in the dark for 30 min. After extracellular staining, cells were washed twice with 200 μL staining buffer.

Cell pellets were resuspended with 100 μL fixation/permeabilization solution and incubated at 4 °C in the dark for 30 min. After fixation and permeabilization, cells were washed twice with 200 μL permeabilization buffer. Cells were then added with 100 μL permeabilization buffer containing Mouse Fc Block (1 μL per well) and incubated at 4 °C in the dark for 5 min. Then, cells were stained with PE-Cy7 FoxP3, PE Ki67 (or isotype) for 30 min at 4 °C in the dark. After antibody incubation, cells were washed twice with permeabilization buffer and resuspended in 200 μL staining buffer, then subjected to flow cytometry within 24 h after staining. Stained cells were acquired on a Cytek Aurora spectral flow cytometer. Fluorescence-Activated Cell Sorting (FACS) data were analyzed using FlowJo software (v10.7.1), SPSS, and GraphPad Prism. A hierarchical gating strategy was employed to identify distinct immune and stem cell-like populations within the TILs, as illustrated in supplementary material (Fig. S1). This strategy sequentially gated on: (1) all acquired events; (2) viable cells (Zombie NIR negative); (3) single cells based on FSC-A vs FSC-H; (4) $CD45^+$ leukocytes; followed by (5) lineage-specific gating: lymphocytes ($CD3^+$) were subdivided into $CD4^+$ T cells, $CD8^+$ T cells, and Tregs (defined as $CD4^+$ $FoxP3^+$); myeloid cells ($CD11b^+$) were analyzed for dendritic cells (DCs, $CD11c^+MHCII^+$), granulocytes ($Ly6C^+/Ly6G^+$), and other subsets; and (6) identification of minor subpopulations including PBMC/MSC, non-classical (NC) cells, and mouse mesenchymal stem/stromal cell (M-MSC) based on their respective marker expression profiles (CD49b, CD69, etc., as defined by the antibody panel) (Fig. S1, a representative example of the hierarchical gating strategy). The reagents used in this study are further described in the supplementary material.

RNA-sequencing

Total RNA was isolated from each thymic sample using the RNAmini kit (Qiagen, Germany). RNA quality was examined by gel electrophoresis and with Qubit (Thermo, Waltham, MA, USA). For RNA sequencing, RNA samples from 7 to 9 biological replicates at each time point (0, 12, 36 and 72 h) were separated into 3 independent pools, each comprised of 2 or 3 distinct samples at equal amounts. Strand-specific libraries were constructed using the TruSeq RNA sample preparation kit (Illumina, San Diego, CA, USA), and sequencing was carried out using the Illumina Novaseq 6000 instrument. Skewer handled the raw data, and data quality was checked using FastQC v0.11.2. The read length was 2×150 bp. Clean reads were aligned to the human genome *hg38* using STAR and StringTie. The expression of the transcript was calculated using Perl and fragments per kilobase of exon model per million mapped reads (FPKM). Differentially expression transcripts (DETs) were determined using the MA-plot-based method with a random sampling (MARS) model in the DEGseq package between different time points. Generally, in the MARS model, $M = \log_2C_1 - \log_2C_2$, and $A = (\log_2C_1 + \log_2C_2)/2$ (C_1 and C_2 denote the counts of reads mapped to a specific gene obtained from two samples). The thresholds for determining DETs are $P < 0.05$ and absolute fold change $\geqslant 2$. Then, DETs were chosen for function and signaling pathway enrichment analysis using Gene Ontology (GO) and Kyoto Encyclopedia of Genes and Genomes (KEGG) databases. The significantly enriched pathways were determined when $P < 0.05$ and at least two affiliated genes were included. PPI analysis of differentially expressed genes was based on the Search Tool for the Retrieval of Interacting Genes/Proteins (STRING) database, which known and predicted protein-protein interactions. The network was established according to the known interaction of the selected reference species. Gene set enrichment analysis (GSEA) is a computational approach to determine if a predefined gene set can show a significant, consistent difference between two biological states. The genes were ranked according to the degree of differential expression in the two samples, and then the predefined gene set was tested to see if they were enriched at the top or bottom of the list. Gene set enrichment analysis can include subtle expression changes. We use the local version of the GSEA analysis tool. Hallmark data sets were used for GSEA independently. Candidate fusion transcripts were identified by STAR-Fusion, which processes the output generated by the STAR aligner to map junction reads and spanning reads to a reference annotation set.

Single-cell RNA-sequencing

Using the 10x Chromium 3' Single Cell platform, we performed scRNA-seq following the manufacturer's protocol. Over 20 000 cells per lane were loaded onto a

chip and partitioned into individual gel beads (GEMs) within the chromium instrument. This was followed by cell lysis, barcoded reverse transcription of RNA within the droplets, emulsion breaking, amplification, fragmentation, and adapter and sample index addition. Pooled libraries were sequenced on the NovaSeq 6000 (PE150) platform. Finally, cDNA and library quality were assessed using the Qubit2.0 Fluorometer. Seurat (version 4.2.0) was used to process single-cell data and perform subsequent analysis. For upper tract urothelial carcinoma (UTUC) and standard ureteral samples, low-quality cells with less than 200 or more than 5000 expressed genes and cells with more than 25% mitochondrial RNA content were filtered out. For BLCA samples from online data sets, low-quality cells with fewer than 400 or more than 5000 expressed genes and cells with more than 10% mitochondrial RNA content were removed. SCTransform, RunPCA, and RunUMAP functions were applied for data normalization and dimensionality reduction. The Harmony (version 0.1.1) package was employed to correct batch effects between arrays. The scHCL (version 0.1.1) and SingleR (version 1.10.0) packages aided in identifying cell subpopulations, and cluster-specific marker genes were identified using the FindAllMarkers function of the Seurat package. Spearman correlations between different cell clusters were calculated using the R package stats Cor function (version 4.2.1) and visualized using the heatmap package (version 1.0.12). To identify malignant cells within ureter and bladder epithelial cell populations, CopyKAT software (version 0.1.0) was utilized to analyze each cell's copy number variation (CNV).

Sample preparation and MSD analysis for cytokines release

Tumor samples need protein extraction and quantification preparation first, then MSD analysis proceeds with serum and tumor samples. STEP 1: Create individual U-PLEX Linker-Coupled antibody solutions. Add 200 µL of each biotinylated antibody to 300 µL of the assigned linker in the Linker vial. Mix by vortexing and incubate at room temperature (RT) for 30 min. Add 200 µL of stop solution. Mix by vortexing and incubate at RT for 30 min. STEP 2: Prepare the multiplex coating solution. Combine 600 µL of each U-PLEX Linker-Coupled antibody solution (10×) into a single tube and vortex. When combining fewer than 10 antibodies, bring the solution up to 6 mL with stop solution. STEP 3: Coat the U-PLEX plate. Add 50 µL of multiplex coating solution to each well, seal the plate with an adhesive plate seal and shake at RT for 1 h. Wash the plate thrice with at least 150 µL/well of 1× MSD wash buffer. STEP 4: Prepare calibrator standards and detection antibody solution. STEP 5: Assay protocol. Add 25 µL of Diluent 43 to each well. Tap the plate gently on all sides. Add 25 µL of the prepared calibrator standard or sample to each well. Seal the plate with an adhesive plate seal. Incubate at RT with shaking for 1 h. Wash the plate thrice with at least 150 µL/well of 1× MSD wash buffer. Add 50 µL of detection antibody solution to each well. Seal the plate with an adhesive plate seal. Incubate at RT with shaking for 1 h. Wash the plate thrice with at least 150 µL/well of 1× MSD wash buffer. Add 150 µL of MSD GLOD Read Buffer B to each well. Analyze the plate on an MSD instrument. Incubation in the read buffer is not required before reading the plate.

Serum and tumor samples from animals were prepared for cytokines release (IFN-γ, IFN-β, TNF-α, GM-CSF, IL-10, IL-2, IL-4, IL-8, MCP-1) by U-PLEX Biomarker Group 1 (mouse) Multiplex assays (MSD U-PLEX Platform). The data were analyzed using MSD Discovery workbench and GraphPad Prism. The reagents used in this study are further described in the supplementary material.

Translocation of DAMPs in tumor cell lines

Harvest tumor cells (H22, EMT6, CT26), count viable cells with Vi-Cell and adjust cell density. Seed 1.8 mL cell solution/well to 6-well flat bottom tissue culture plate according to the plate map to make the cell confluence at 80%−90%. Prepare 1000× compound solution in DMSO, then 100-fold dilution with growth medium to make 10× compound solution, add 0.2 mL of 10× drug solution into corresponding wells, the final concentration is 10 µmol/L, 1 µmol/L and 0.1 µmol/L. Add 0.2 mL 1% DMSO solution to the vehicle control wells, diluted in culture medium. Add 0.2 mL of culture medium to cell-only wells. Incubate the cells in a humidified incubator at 37 °C with 5% CO_2 for 24 h and 48 h. Centrifuge the plates at 1500 rpm for 5 min, transfer 1 mL supernatant per well from each plate, and transfer the supernatant for HMGB-1 detection by ELISA. Remove the residual supernatant to a new plate, wash cells with PBS, dissociate cells with TrypLE and pool all cells together (in the supernatant, in the PBS washing solution and the dissociated cells) from the same well, transfer cells for FACS analysis. The supplementary material further describe the reagents used in this study and assay procedures.

Procedures and equipment

The experimental procedures, equipment, and reagents used in this study are detailed in the supplemental materials document.

Results

FNC exhibits anti-tumor effects on solid tumor cells dependent on an intact immune system

The primary objective of this study was to evaluate whether FNC can exhibit cytotoxic or inhibitory effects on solid tumor cells both *in vitro* and *in vivo* and to systematically assess its impact on the commonly observed immunosuppressive local microenvironment in solid tumors. We used three commonly studied tumor cell lines —H22 (hepatocellular carcinoma), EMT6 (breast cancer), and CT26 (colorectal cancer)—to establish tumor models. CT26 models were developed in both immunocompetent and immune-depleted mice to compare immune-dependent anti-tumor effects. Various detection methods, including scRNA-seq, RNA-seq, and MSD, were employed to systematically evaluate the regulatory effects of FNC on CT26 tumors and their microenvironment (Fig. 1A). The *in vitro* results indicated that FNC partly inhibited the proliferation of colorectal cancer, breast cancer, and hepatocellular carcinoma cells in a time- and dose-dependent manner. At 24 h and 48 h of incubation, FNC demonstrated superior IC_{50} indices in inhibiting the proliferation of the three tumor cell types compared to cisplatin (serving as a positive control) (Fig. 1B−1D), with IC_{50} indices further decreasing with extended incubation times (Fig. 1E). These findings are consistent with previous reports indicating that FNC exhibits anti-tumor effects even at low concentrations. However, compared to typical cytotoxic chemotherapeutic agents such as cisplatin, the cytotoxic effects of low-concentration FNC on tumor cells remain relatively limited.

Subsequently, we evaluated whether the potential anti-tumor effects exhibited by FNC depend on an intact

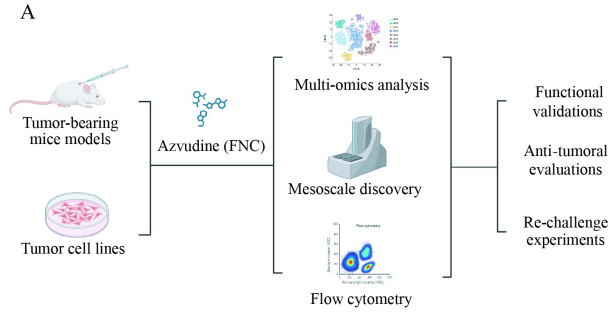

E

Cell lines	24 h		48 h	
	FNC	Cisplatin	FNC	Cisplatin
CT26	>10 μmol/L	15.764 μmol/L	0.15 μmol/L	2.899 μmol/L
EMT-6	6.55 μmol/L	7.591 μmol/L	0.41 μmol/L	1.939 μmol/L
H22	2.68 μmol/L	4.476 μmol/L	0.06 μmol/L	1.51 μmol/L

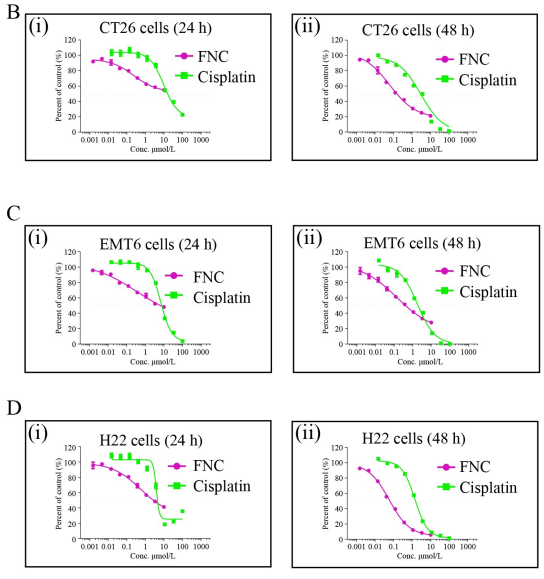

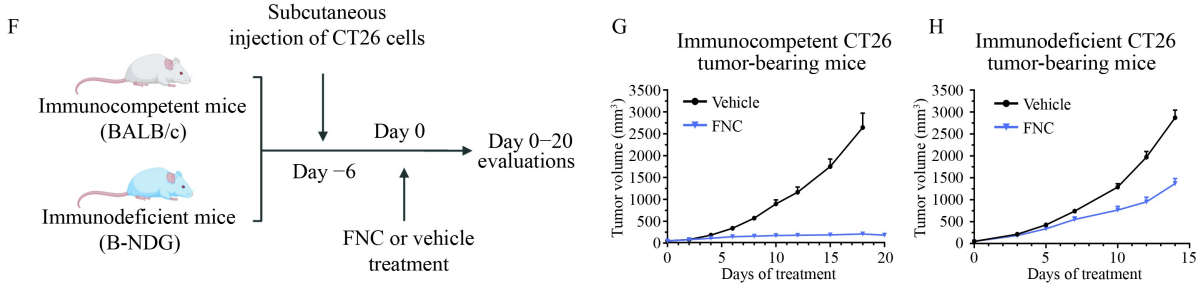

Fig. 1 Overall study design and evaluation of the anti-tumor effects of FNC *in vitro* and *in vivo*. (A) Schematic representation of the intervention and evaluation strategies of FNC on syngeneic tumor-bearing mouse models and tumor cell lines *in vitro*. (B−D) Exploration of the anti-tumor effects and optimal effective concentrations of FNC on (B) CT26, (C) EMT6, and (D) H22 cell lines *in vitro*. (E) Assessment of the time- and dose-dependent anti-tumor effects of FNC on CT26, EMT6, and H22 cell lines *in vitro*. (F) Schematic illustration of the construction and evaluation of syngeneic tumor-bearing mice treated with FNC under immunocompetent and immunodeficient conditions. (G) Dynamic changes in tumor volume in immunocompetent tumor-bearing mice treated with FNC. (H) Dynamic changes in tumor volume in immunodeficient tumor-bearing mice treated with FNC. (I–K) Exploration of the anti-tumor effects and optimal effective concentrations of FNC on syngeneic tumor-bearing mice constructed with (I) CT26, (J) EMT6, and (K) H22 cell lines *in vivo*.

immune system, mainly focusing on the immune cells infiltrating the TME. To this end, we further examined the anti-tumor effects of FNC in both immunocompetent and immunodeficient backgrounds (Fig. 1F). Interestingly, in immunocompetent tumor-bearing mice, 1 mg/kg FNC produced a highly effective and sustained inhibitory effect on tumor growth (Fig. 1G). In contrast, in the context of a microenvironment lacking immune effector cells (such as T cells and NK cells), the inhibitory effect of FNC on tumor cells was significantly impaired (Fig. 1H). These results further suggest that the anti-tumor effects of FNC largely depend on an intact host immune system or, more reasonably, on its ability to regulate and activate host immunity, as supported by enhanced immune cell infiltration and immune pathway activation.

As validation of this hypothesis, FNC exhibited significant inhibitory effects on tumor growth in multiple solid tumor-bearing mouse models constructed using immunocompetent mice. These models were established by subcutaneously injecting varying numbers of tumor cells into the mice. The CT26, H22, and EMT6 cells were successfully implanted in immunocompetent mice, forming tumors of 50−100 mm^3. According to the random grouping strategy, tumor-bearing mice received daily oral treatment with FNC at either 0.5 mg/kg, 1 mg/kg, or saline. Results showed that although FNC treatment at 0.5 mg/kg slowed tumor growth in tumor-bearing mice compared to the control group (Fig. 1I−J), NC treatment at 1 mg/kg exhibited significant anti-tumor effects in tumor-bearing mice. Around day 15 after treatment initiation, the median volumes of CT26, H22, and EMT6 tumors began to shrink. By day 27, 4 out of 10 mice in each treatment group exhibited complete tumor regression, defined as undetectable tumor volume upon palpation and caliper measurement. However, although the tumor volume in the remaining mice decreased after treatment cessation, tumor growth resumed around day 38−day 40.

RNA-seq analysis of tumor tissues from tumor-bearing mice (CT26) indicated that 1 mg/kg FNC treatment significantly altered the transcriptomic characteristics of the tumors. Based on the predefined threshold, differential gene expression analysis identified 1461 differentially expressed genes (DEGs), with 891 upregulated and 570 downregulated (Fig. 2A). Functional annotation of these DEGs revealed that FNC significantly activated immune activation and downstream signaling pathways (Fig. 2B). Corresponding to the previously observed *in vivo* and *in vitro* anti-tumor effects, the GSEA analysis indicated that FNC treatment induced significant apoptotic phenotypes in tumor cells (Fig. 2C). These findings suggest that the anti-tumor effects of FNC may be closely related to its potential regulatory effects on the tumor immune microenvironment.

FNC remodels the local immunosuppressive microenvironment of tumors across multiple omics dimensions

Previous studies have reported that an immunosuppressive local TME contributes to cancer progression and drug resistance by fostering diverse, resistant subclones and supporting immune evasion mechanisms. In light of *in vivo* experiments suggesting that FNC's anti-tumor effects are dependent on immune modulation, we utilized scRNA-seq technology to investigate the regulatory effects of FNC on the TME at the single-cell level. Through scRNA-seq and rigorous bioinformatics quality control and analysis of tumor tissues from syngeneic tumor-bearing mice, we successfully obtained a total of 51 924 single-cell transcriptomes from FNC-treated (n = 3) and control (n = 3) mouse tumor tissues. Annotations of these heterogeneous cell subpopulations on the t-SNE plots revealed no significant differences in the cellular composition (Fig. 3A). By annotating transcriptional characteristics of various cell subpopulations, we successfully identified 18 immune cell subpopulations, including $CD8^+$ CTLs, B lymphocytes, and NK cells (Fig. 3B).

An in-depth analysis of these immune cell subpopulations indicated that FNC profoundly altered the proportional distribution of infiltrating immune cells in tumor tissues. Compared to the control group, FNC treatment significantly increased the proportions of memory T cells, NK cells, and $CD8^+$ CTLs in the local TME of tumor-bearing mice while significantly reducing the proportions of immunosuppressive M2 macrophages and M-MDSCs (Fig. 3C). Consistent with the dynamic trends observed in the immune cell subpopulations, an analysis of intercellular communication among tumor-infiltrating immune cells post-FNC treatment demonstrated that FNC significantly modulated the interactions between immunoregulatory cells (such as MDSCs and M2 macrophages) and effector immune cells (such as $CD8^+$ CTLs and NK cells), both in terms of communication frequency (Fig. 3D) and intensity (Fig. 3E). Interestingly, although FNC exhibited a certain degree of *in vivo* anti-tumor effect, the high activation of immune checkpoint pathways and downstream transcriptomes in the FNC-treated tumor tissues suggests the presence of an immune tolerance mechanism dependent on immune checkpoint proteins in the local TME in MDSCs (Fig. 3F). These results confirm the regulatory effects of FNC on the local immunosuppressive microenvironment of tumors and further support the rationale for combining FNC with immune checkpoint blockade strategies to enhance its anti-tumor effects. This single-cell analysis of tumor tissues before and after FNC treatment reveals that FNC

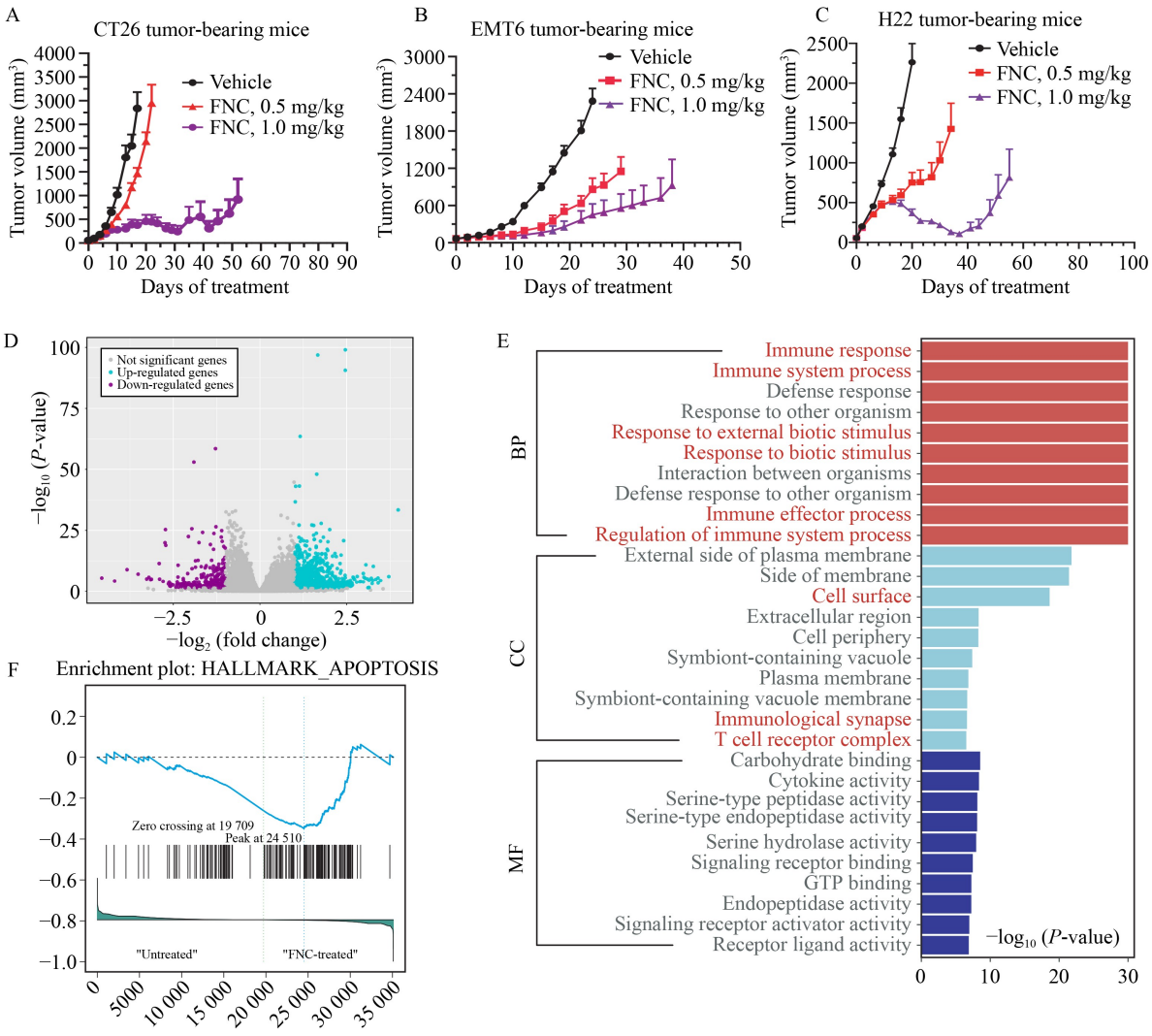

Fig. 2 Exploration of the molecular pathways FNC targets and assessment of its immune-dependent anti-tumor effects *in vivo*. (A) Identification and volcano plot presentation of DEGs in FNC-treated vs. CT26 tumor bearing mice. Differential gene expression analysis identified 1461 DEGs, with 891 upregulated and 570 downregulated. (B) Functional annotation of the DEGs identified in FNC-treated CT26 tumor bearing mice. Red terms indicate significantly enriched immune-related pathways. (C) GSEA of DEGs identified in FNC-treated CT26 tumor bearing mice showed significant apoptotic pathways enrichment in FNC-treated CT26 cells.

significantly reduces MDSC infiltration while increasing the infiltration of effector T and NK cells. At the molecular level, FNC regulates checkpoint-related signaling pathways, potentially increasing the presentation of tumor-specific antigens.

To further validate the impact of FNC on the TME, we utilized flow cytometry to examine the cellular composition and secretion factors within the microenvironment of immunocompetent CT26 tumor-bearing mice treated with various doses of FNC. Utilizing a 12-color flow cytometry panel, at least 50 000 $CD45^+$ tumor tissue suspension cells were obtained from each sample for immune cell subset analysis (Fig. 4A). Our data confirmed that FNC increased the infiltration of total T cells, $CD8^+$ CTLs, and NK cells in tumor tissues (Fig. 4B−4D). Simultaneously, FNC markedly elevated the $CD8^+$ T cell/Treg ratio, suggesting enhanced cytotoxic immune responses and reduced immunosuppressive dominance within the TME (Fig. 4E). Additionally, the proportions of immunosuppressive M-MDSCs and PMN-MDSCs, which play a significant negative regulatory role in cellular immunity, were notably reduced in the FNC-treated microenvironment (Fig. 4F and 4G).

FNC inhibits tumor cells by activating the ICD-DAMP axis and remodeling the secretory phenotype

The previous findings have clarified that FNC mediates its anti-tumor effects by activating apoptosis-related molecular signatures in tumor cells (Fig. 1B−1D and Fig. 2F). It is noteworthy that, although apoptosis is

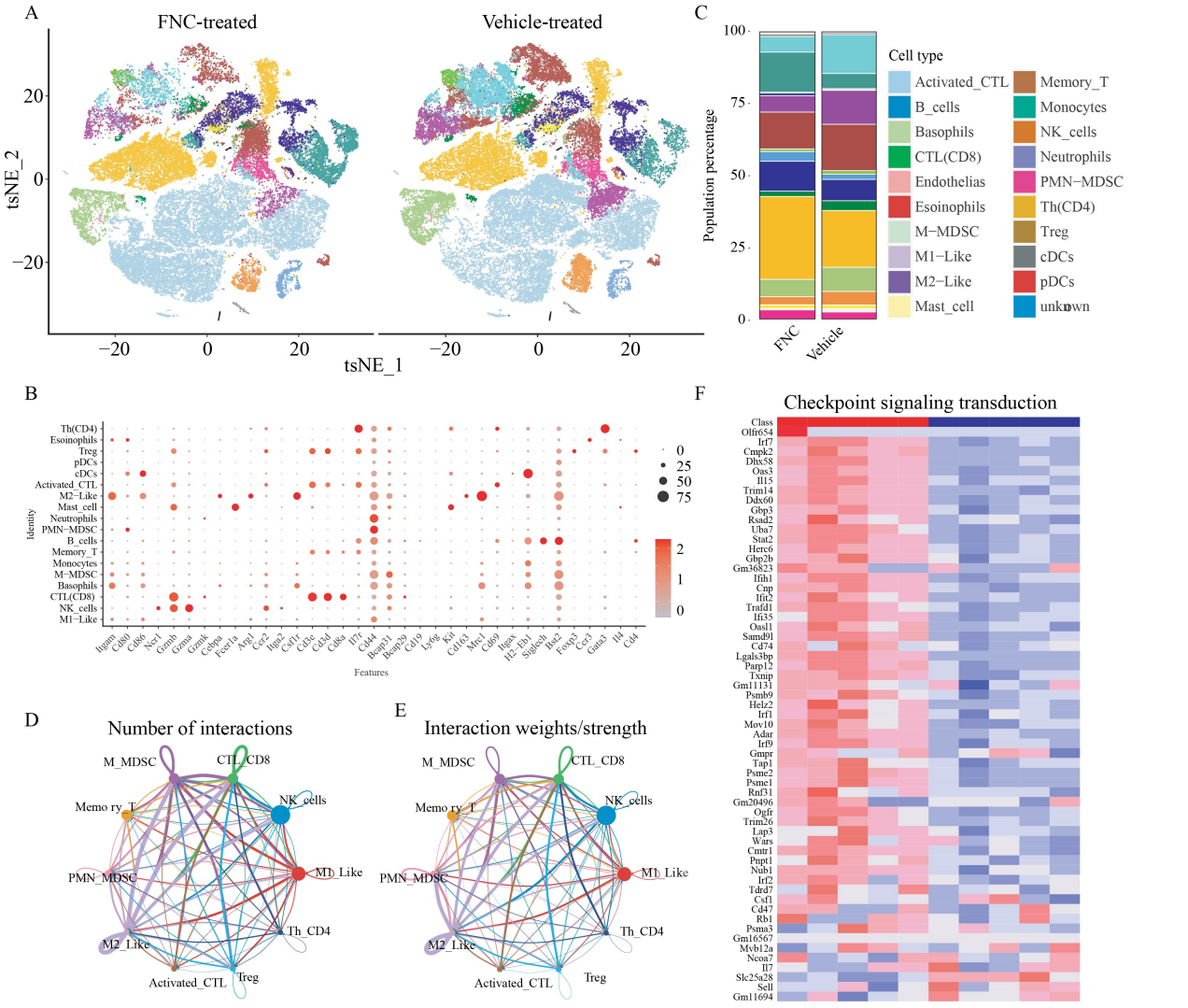

Fig. 3 Single-cell molecular analysis of the local TME in CT26 tumor-bearing mice. (A) tSNE plot showing the single-cell molecular analysis of the local TME in CT26 tumor-bearing mice. (B) Molecular annotation of immune cell subsets in the local TME of CT26 tumor-bearing mice. (C) Quantitative statistics of immune cell subsets in the local TME of CT26 tumor-bearing mice. (D, E) Quantitative statistics of intercellular communication (D) quantity and (E) intensity among immune cells in the local TME of CT26 tumor-bearing mice. (F) Heatmap showing the expression levels of immune checkpoint-related transcripts in infiltrating MDSCs in the TME.

traditionally considered a form of cell death that does not elicit a significant immune response, specific immunogenic cell death (ICD) induction pathways can convert this process into an immunogenic form of cell death, thereby enhancing anti-tumor immune responses [12]. During ICD, DAMPs induced by stressed dying cells translocate and are released. DAMPs such as ATP, calreticulin (CRT), high-mobility group box 1 (HMGB1), and heat shock proteins (HSPs) translocate from inside the cell to the cell surface or are released extracellularly, activating antigen-presenting cells (APCs). APCs recognize these damage-associated molecular patterns (DAMPs), phagocytize dying cells, present antigens, and activate immune cells, ultimately eliciting a potent anti-tumor immune response. MSD technology identified a dose- and time-dependent upregulation of DAMP molecules, including CRT, Annexin A1, and HSP90, in FNC-treated colorectal cancer cells (Fig. 5A−5H). HMGB1 acts as a DAMP during ICD by translocating from the nucleus to the extracellular space, activating immune responses, inducing dendritic cell maturation, promoting antigen presentation, and ultimately eliciting effective anti-tumor immunity. In H22 cell lines, FNC at concentrations ranging from 0.1 to 10 μmol/L significantly upregulated HMGB1 expression in tumor cells, whereas EMT6 and CT26 cell lines required 10 μmol/L FNC to upregulate HMGB1 expression (Fig. 5I−5K) significantly. These results confirm that FNC promotes the exposure of tumor-specific DAMPs and suggest that different types of cancer cells may have

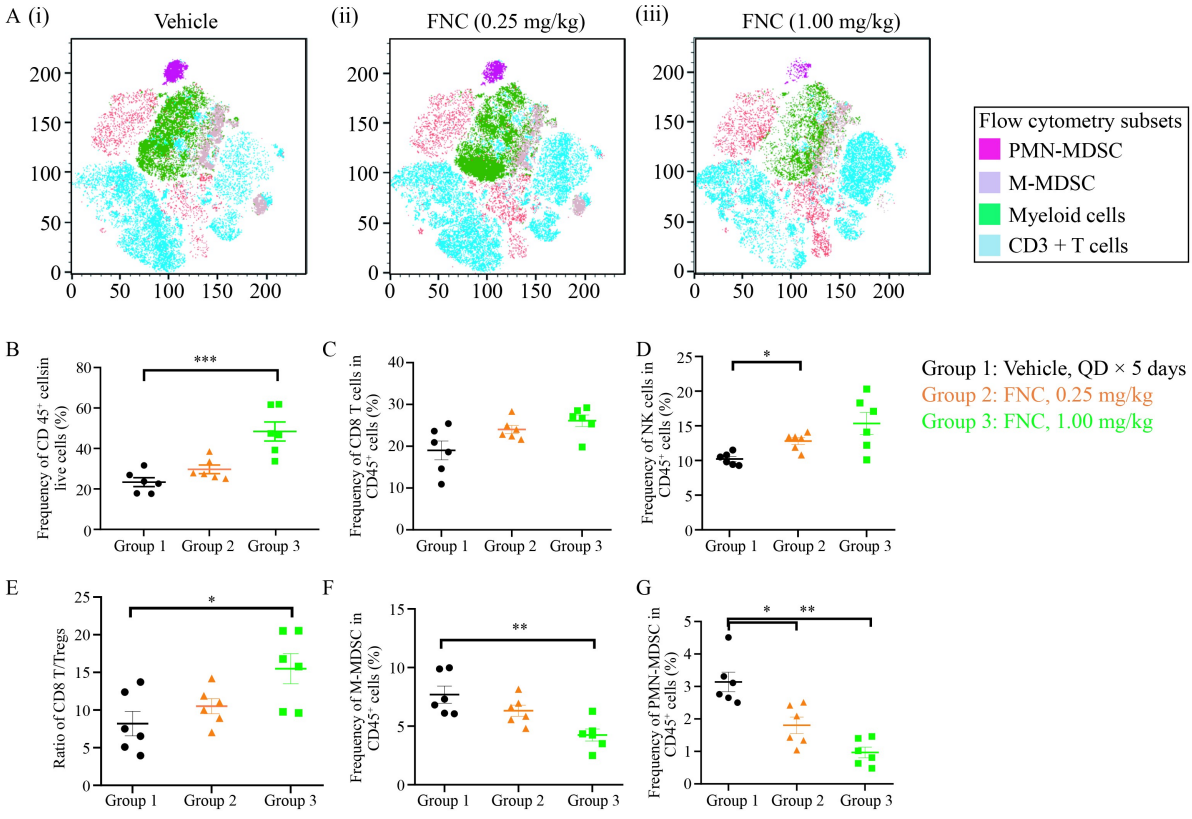

Fig. 4 Flow cytometric identification of immune cell surface antigens in the local TME of CT26 tumor-bearing mice. (A) tSNE plot showing immune cell subsets among 50 000 selected $CD45^+$ cells. (B–G) Flow cytometric statistics of the quantities of (B) $CD45^+$ cells, (C) $CD8^+$ T cells, (D) NK cells, (E) $CD8^+$ T cell/Treg ratio, (F) M-MDSCs, and (G) PMN-MDSCs in the local TME.

varying sensitivities and susceptibilities to FNC.

The activation of the ICD-DAMP axis is also accompanied by a dose-dependent release of pro-inflammatory cytokines in the TME in response to FNC. FNC exhibited a potential upregulating effect on the levels of IFN-γ, TNF-α, and IL-2 within tumor tissues *in vivo* (Fig. 6A–6C), suggesting that FNC may enhance anti-tumor immune responses by activating macrophages, enhancing antigen presentation, and promoting Th1-type immune responses. These changes may contribute to converting cold tumors into hot tumors, thereby improving the responsiveness of tumors to immunotherapy. IL-4 levels showed a decreasing trend in tumor tissues at the 1 mg/kg dose, although this was not statistically significant, indicating that FNC may partially alleviate IL-4-mediated immunosuppression (Fig. 6D). There were no significant changes in the levels of IL-8 and IL-10, further supporting the notion that FNC primarily exerts its effects through the activation of immune factors rather than the broad inhibition of immunosuppressive factors (Fig. 6E and 6F). FNC exerted bidirectional trends without reaching statistical significance on the levels of MCP-1, GM-CSF, and IFN-β in tumor tissues, suggesting that it potentially influences the recruitment, maturation, and function of immune cells, supporting the potential mechanism of FNC in combating tumors through enhanced immune activation (Fig. 6G–6I). These results suggest that the upregulation of DAMP expression, under FNC intervention, further activates the ICD process in tumor cells.

FNC combined with anti-PD-1 therapy exhibits synergistic and durable anti-tumor effects

Given FNC's dependence on an intact immune system for its anti-tumor effects and its activation of the tumor-local immune microenvironment, we further investigated whether combining FNC with immune checkpoint inhibitor therapy could yield synergistic and superior anti-tumor effects (Fig. 7A). Drug intervention experiments in tumor-bearing mice indicated that anti-PD-1 monotherapy did not significantly delay the growth of CT26 tumors compared to the control group (Fig. 7B, green). Consistent with previous observations, FNC monotherapy exhibited notable anti-tumor effects, significantly inhibiting tumor growth and resulting in complete tumor regression in 4 out of 10 treated mice (Fig. 7B, purple). Interestingly, in the combination therapy group (FNC + anti-PD-1), complete tumor regression was observed in all mice within 39 days of treatment initiation (Fig. 7B, blue).

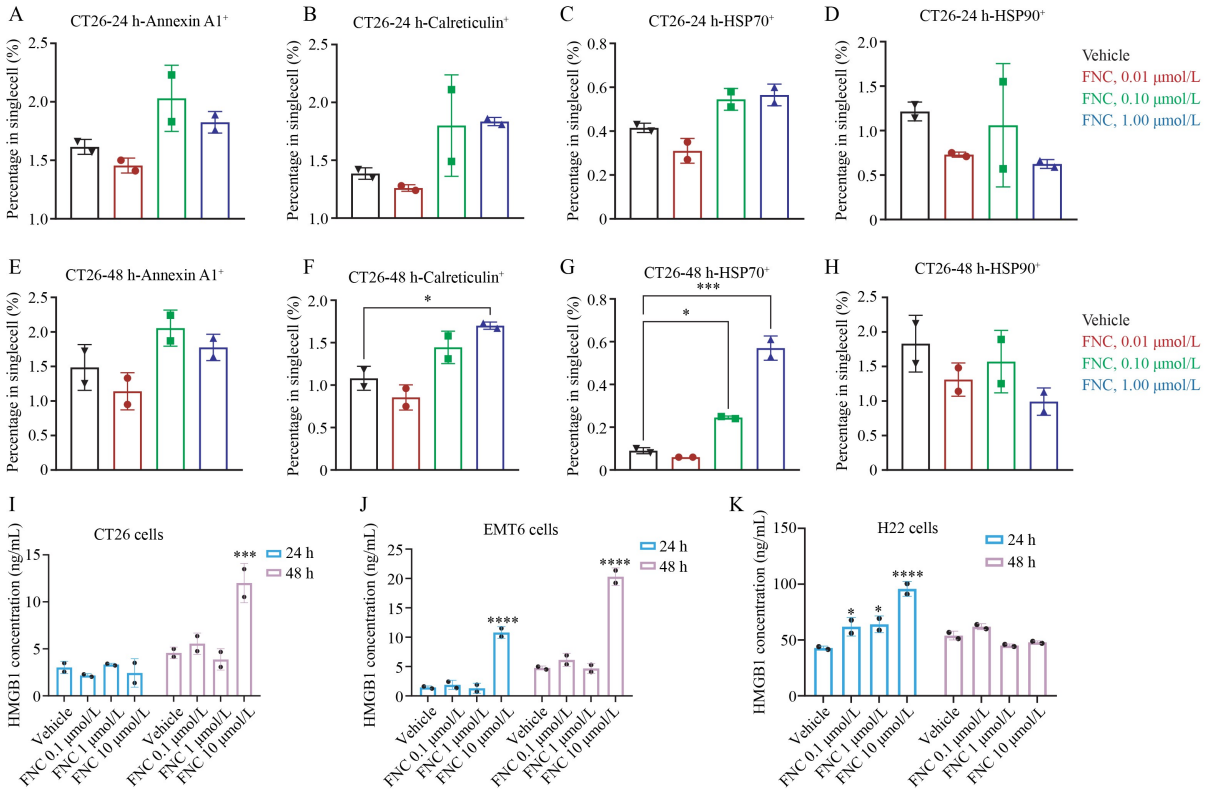

Fig. 5 Evaluation of the regulation of ICD and DAMP-related molecular markers in FNC-treated CT26 tumor cells. (A−D) Flow cytometric assessment of the expression levels of (A) Annexin A1, (B) Calreticulin, (C) HSP70, and (D) HSP90 in tumor cells pretreated with different concentrations of FNC for 24 h. (E−H) Flow cytometric assessment of the expression levels of (E) Annexin A1, (F) Calreticulin, (G) HSP70, and (H) HSP90 in tumor cells pretreated with different concentrations of FNC for 48 h. (I−K) Evaluation of the expression levels of HMGB1 transcripts in (I) CT26, (J) EMT6, and (K) H22 cell lines treated with different concentrations of FNC.

Consistent with these observations, the combination therapy group exhibited superior overall survival following tumor cell inoculation, with no tumor relapse noted until the last follow-up on day 88 (Fig. 7C). To assess the persistence of FNC-mediated anti-tumor effects *in vivo*, a re-challenge experiment was conducted on another cohort of tumor-free mice following FNC pretreatment/therapy (Fig. 7A). The results showed that mice tumor-free after either single-agent FNC intervention or FNC combined with PD-1 monoclonal antibody intervention did not develop subcutaneous tumors upon re-challenge with tumor cells (Fig. 7D). This long-term tumor inhibition after FNC discontinuation was accompanied by a significant increase in total T cells, T helper cells, CTLs, effector T cells, and effector memory T cells in peripheral blood (Fig. 7E). These findings suggest that FNC can activate the host immune system to exert a long-term anti-tumor effect.

FNC implicates PD-1 signaling as a central transcriptional hub in tumor immune regulation

Comprehensive pathway enrichment analysis of differentially expressed genes following treatment revealed profound alterations in immune regulatory networks within the TME. Fig. 8A enumerates key enriched biological processes, including translocation of ZAP-70 to immunological system, activation, myristolization of BID and translocation to mitochondria, activation of C3 and C5, PD-1 signaling, phosphorylation of CD3 and TCR ζ chain, and downstream TCR signaling, among others. Quantitative assessment of pathway significance (Fig. 8B) confirmed that PD-1 signaling was the most significantly enriched term, exhibiting an exceptionally low *P*-value ($-\log_{10}$(*P*-value) ≈12).

This finding was robustly validated via Reactome pathway analysis. Fig. 8C and 8D consistently ranked PD-1 signaling as the top enriched pathway, demonstrating both the highest statistical significance ($-\log_{10}$(*P*-value) ≈ 12) and a substantial Rich factor (> 0.4), indicating strong over-representation of pathway genes. Critically, Fig. 8E revealed that PD-1 signaling accounted for the largest proportion of pathway-associated genes (≈50%), further underscoring its dominance in the transcriptional landscape.

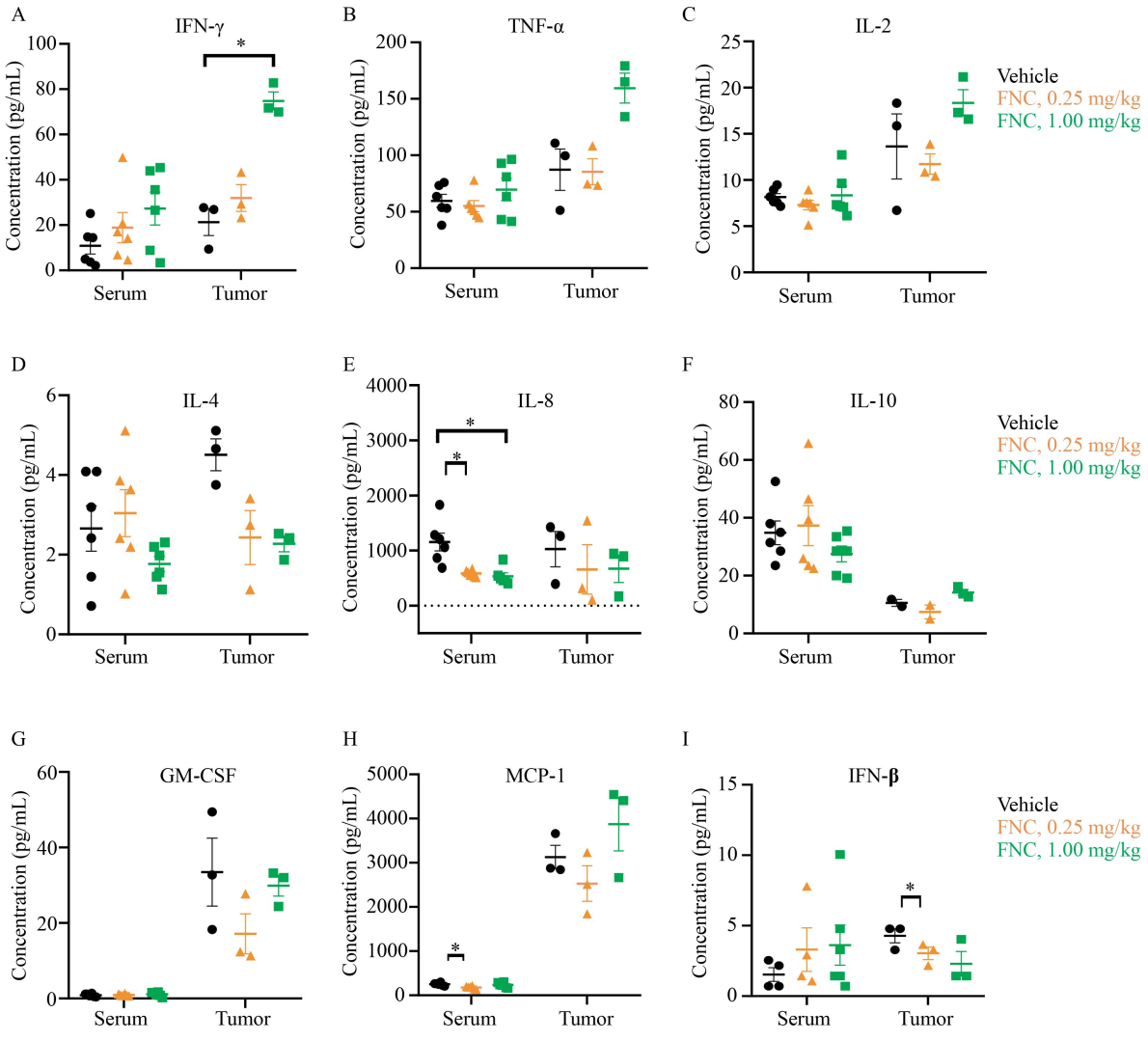

Fig. 6 Evaluation of cytokine regulation in FNC-treated CT26 tumor cells. (A–C) Assessment of the expression levels of (A) IFN-γ, (B) TNF-α, and (C) IL-2 in tumor cells pretreated with different concentrations of FNC. (D–F) Assessment of the expression levels of (D) IL-4, (E) IL-8, and (F) IL-10 in tumor cells pretreated with different concentrations of FNC. (G–I) Assessment of the expression levels of (G) GM-CSF, (H) MCP-1, and (I) IFN-β in tumor cells pretreated with different concentrations of FNC.

Discussion

In our current study, we have revealed for the first time that FNC's anti-tumor effects primarily depend on the immune system. Previous research indicates that FNC exerts significant regulatory effects on various immune system components. In SARS-CoV-2 infected monkeys, FNC treatment primarily increased the proportion of $CD3^+$, $CD4^+$, and $CD8^+$ cells in peripheral blood and thymus [13], suggesting a relationship with MDSCs that requires further experimental investigation. Notably, the Centre for Drug Evaluation in China has approved the use of FNC for treating COVID-19 and AIDS, demonstrating substantial clinical efficacy and safety in patients [14–17], which might facilitate its clinical utilization in combination with anti-PD-1 therapy. Based on the undeniable interaction between FNC and the immune system, it is of potential clinical value to assess whether FNC possesses a regulatory capability over the immune system of tumor-bearing hosts, thereby enhancing the anti-tumor effects that rely on immune-mediated cytotoxicity.

Furthermore, previous studies indicate that tumors modulate the local immune microenvironment and induce the infiltration of immunosuppressive TILs, creating an immunosuppressive microenvironment. This environment impedes the infiltration and cytotoxic effects of effector immune cells such as CTLs and NK cells. Within the TME, MDSCs collaborate with other immune cells and utilize various mechanisms to achieve immunosuppression [5]. The mechanisms include impeding lymphocyte homing, activating immunosuppressive cells, generating

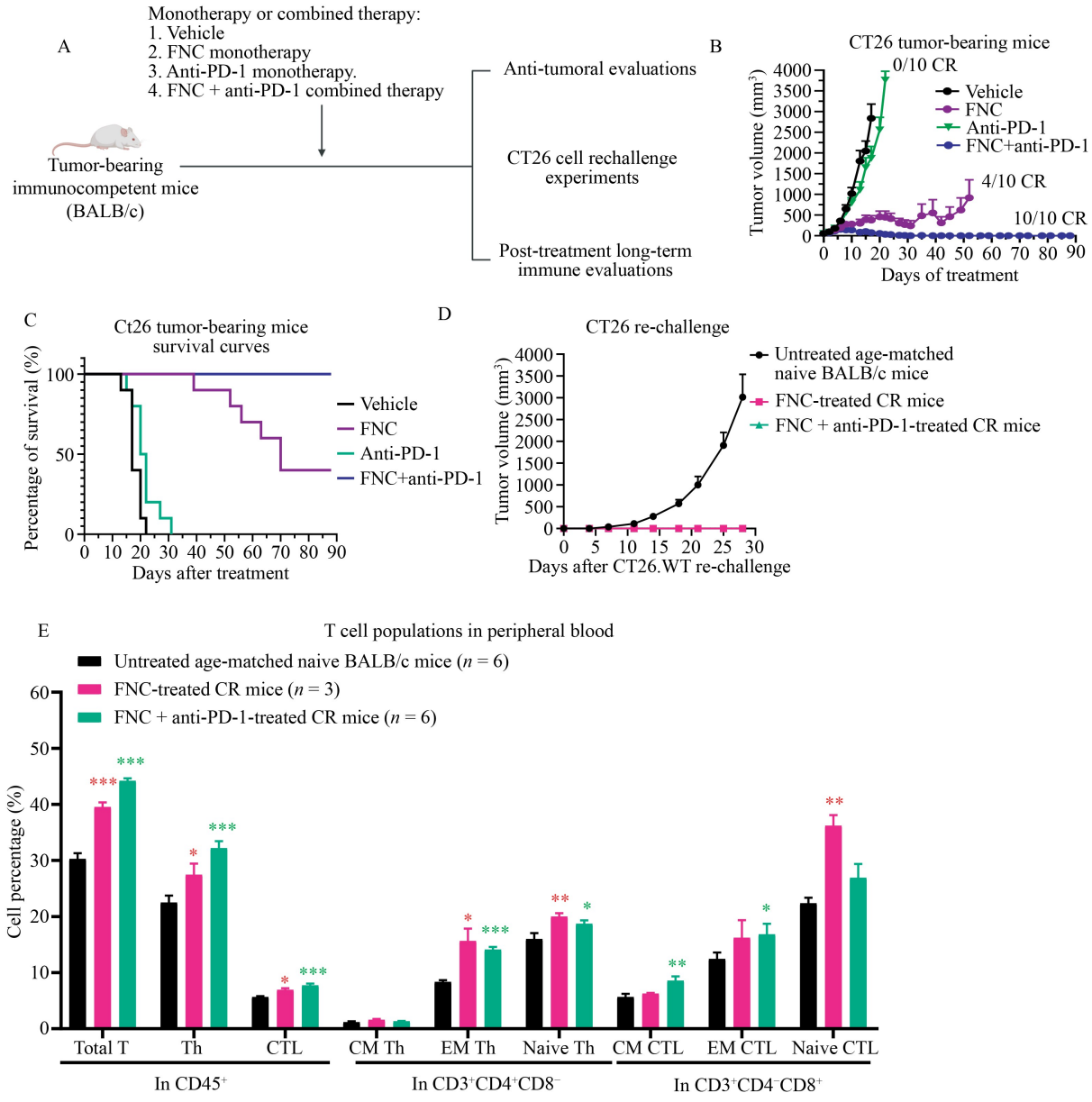

Fig. 7 Evaluation of the anti-tumor effects and durability of combined FNC and anti-PD-1 therapy. (A) Schematic illustration of the evaluation of anti-tumor effects of FNC monotherapy or combined anti-PD-1 monoclonal antibody therapy in immunocompetent tumor-bearing mice. (B) Assessment of tumor volume in tumor-bearing mice treated with FNC monotherapy or combined anti-PD-1 monoclonal antibody therapy. (C) Evaluation of survival time in tumor-bearing mice treated with FNC monotherapy or combined anti-PD-1 monoclonal antibody therapy. (D) Assessment of CT26 re-challenge in tumor-bearing mice that achieved complete regression (CR) following FNC monotherapy or combined FNC and anti-PD-1 therapy. (E) Flow cytometric evaluation of T cell subsets in peripheral blood of tumor-bearing mice that achieved CR following FNC monotherapy or combined FNC and anti-PD-1 therapy. Note: **indicates comparison between the FNC monotherapy group and the anti-PD-1 monotherapy group, $P < 0.01$; ***indicates comparison between the combination therapy group and the FNC monotherapy group, $P < 0.001$; ###indicates comparison between the combination therapy group and the anti-PD-1 monotherapy group, $P < 0.001$.

reactive oxygen species and nitrogen, depleting essential T cell metabolites, expressing exterior enzymes that regulate adenosine metabolism, and expressing damaging immune checkpoint molecules [18]. Recently, MDSCs have been recognized for their critical roles in immune regulation and effectively inhibiting effector lymphocytes' activity [19].

Based on the findings above, evaluating whether FNC exerts its anti-tumor effects in tumor-bearing mouse models is of particular value by remodeling the immunosuppressive local TME. Utilizing various omics techniques, our study revealed that FNC treatment significantly remodels the TME by increasing the infiltration and activity of effector immune cells such as

memory T cells, NK cells, and $CD8^+$ CTLs. Simultaneously, FNC reduces the proportion of immunosuppressive cells, particularly MDSCs and M2 macrophages. These changes suggest that FNC can convert a "cold" TME poorly infiltrated by immune cells into a "hot" TME more amenable to immune attack. Single-cell transcriptomic analysis further revealed that FNC primarily regulates the MDSCs subpopulations and the intercellular communication with various effector T cells and NK cells. This finding suggests that FNC may facilitate the activation of positive immune signals by weakening the inhibitory signals transmitted by MDSCs to the local microenvironment. As another manifestation of FNC's regulatory effects on intercellular communication within the microenvironment, the transduction of immune checkpoint signaling in tumor

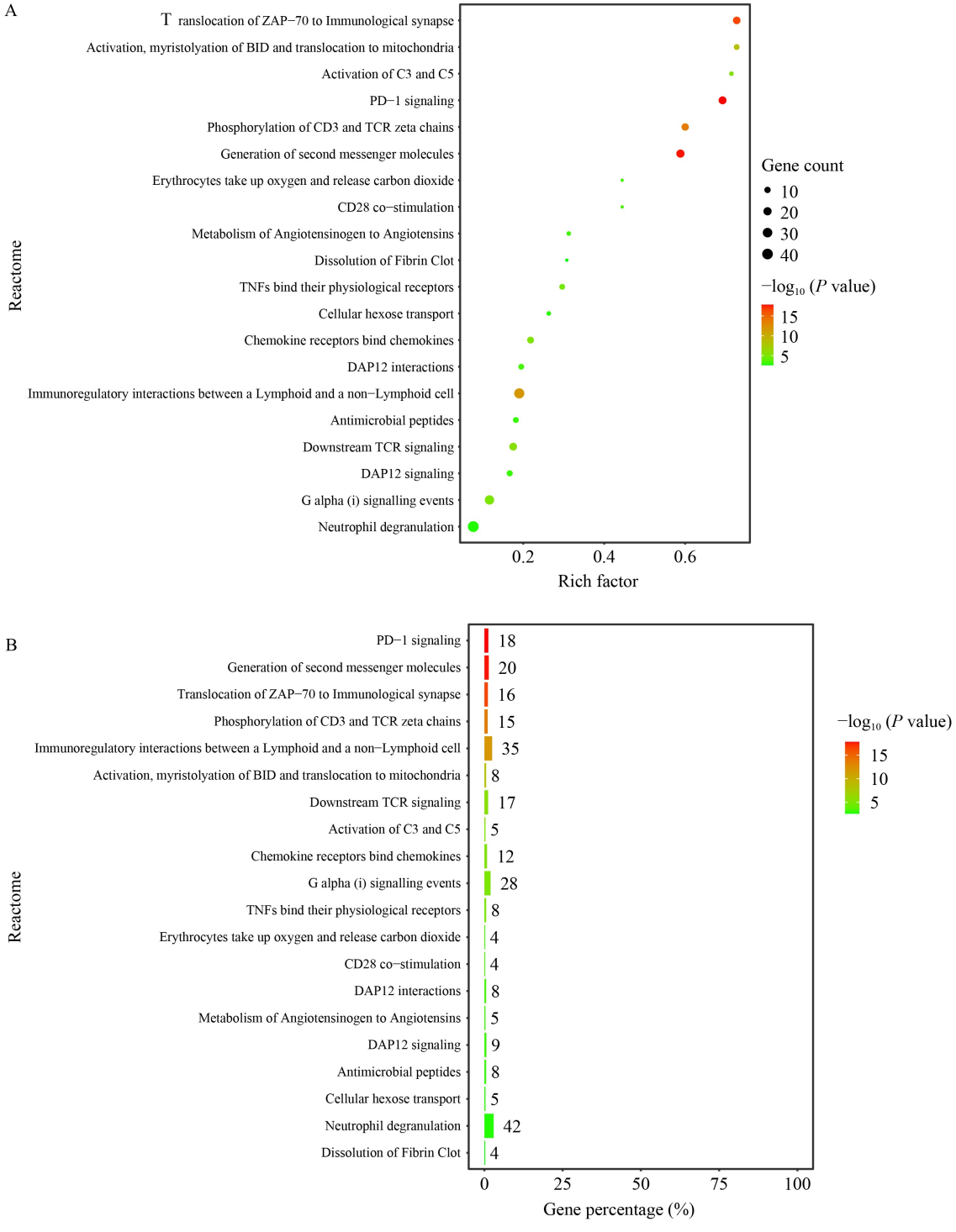

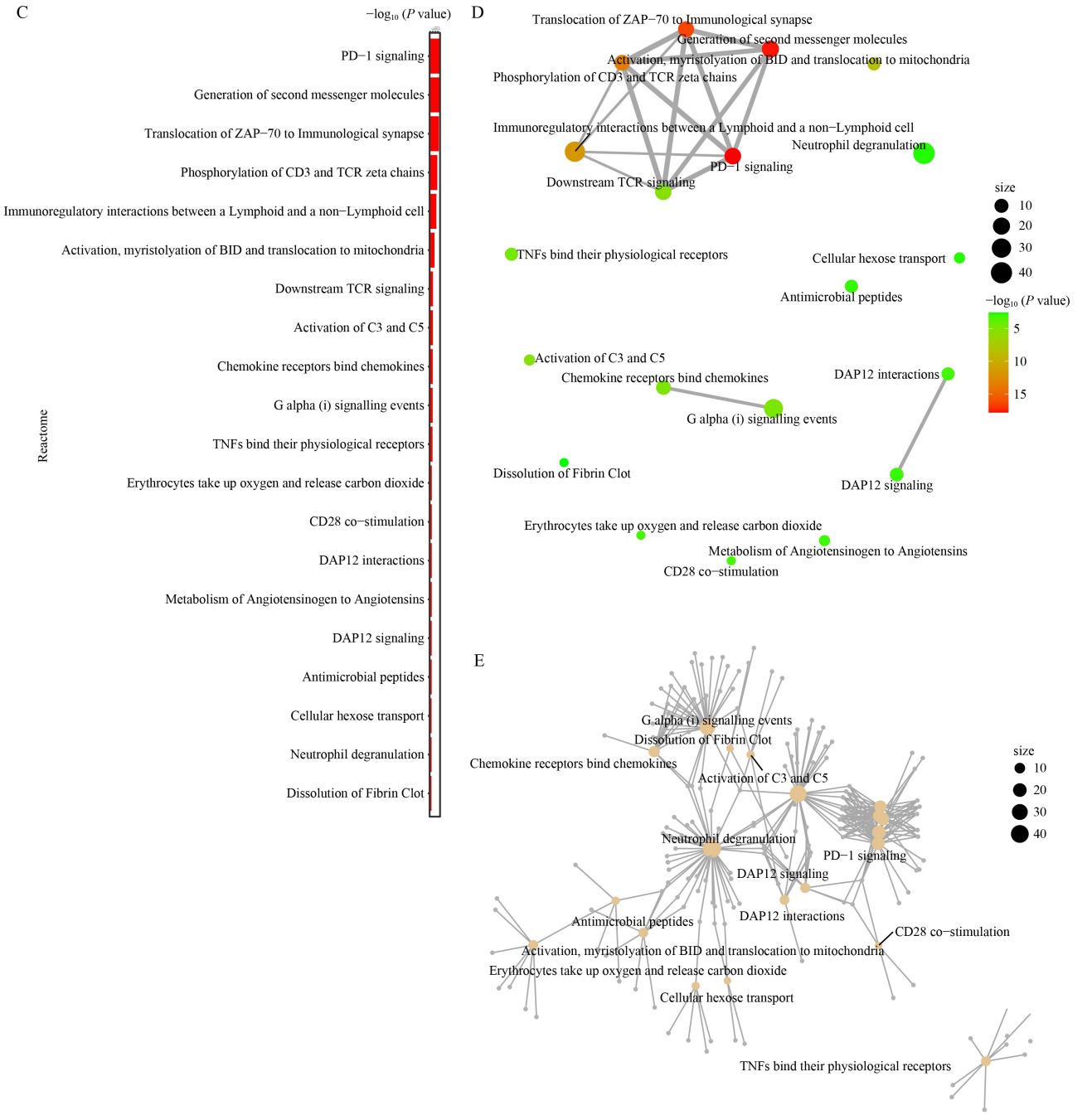

Fig. 8 Transcriptional reprogramming of immune checkpoint and signaling pathways by FNC in the TME. (A) Key enriched biological processes from pathway analysis. (B) Scatter plot of pathway enrichment significance ($-\log_{10}$(*P*-value)) versus gene count. PD-1 signaling (red dot) shows the highest statistical significance ($-\log_{10}$(*P*-value) ≈ 12). (C) Reactome pathway enrichment: ich factor versus $-\log_{10}$(*P*-value). PD-1 signaling (top) exhibits maximal statistical significance ($-\log_{10}$(*P*-value) ≈ 12) and high biological relevance (Rich factor > 0.4). (D) Reactome pathway enrichment: Rich factor versus $-\log_{10}$(*P*-value). Consistent with (C), PD-1 signaling (top) dominates in both statistical and functional enrichment. (E) Pathway gene contribution: PD-1 signaling accounts for ~50% of genes in enriched pathways, confirming its transcriptional dominance.

cells was also inhibited. Notably, this regulatory effect of FNC on the microenvironment components did not directly interfere with the expression levels of classical immune checkpoint proteins such as PD-L1 and TIM-3, suggesting that FNC acts through mechanisms that complement rather than overlap with classical checkpoint blockade pathways.

Our data show that FNC induces ICD, marked by releasing DAMPs such as HMGB1 and CRT. The activation of ICD pathways is crucial as it promotes the recruitment and activation of APCs, thereby enhancing the presentation of tumor antigens and stimulating robust

anti-tumor immune responses [20,21]. This suggests a synergistic effect may be achieved by concurrently remodeling the TME through FNC-induced mechanisms and augmenting ICD for cancer treatment. Consistent with our findings, cutting-edge research has proposed novel treatments that enhance the ICD immune response and diminish the MDSC population. These advancements highlight the potential for combining FNC with strategies that target both the immunogenic pathways and the suppressive components of the TME to achieve more effective cancer therapies [22–24]. Further research is needed to assess whether released DAMPs can stimulate the ability of APCs to effectively cross-prime CTLs and thereby initiate an adaptive immune response.

Notably, complete regression (CR) was achieved in all 10 mice bearing H22 or CT26 tumors treated with FNC plus anti-PD-1, with H22 or CT26 tumors treated with FNC plus anti-PD-1, without any tumor recurrence during the study. This synergy is likely due to the following mechanisms: (1) Reducing the immunosuppressive MDSC population enhances the efficacy of immune checkpoint inhibitors (ICIs) like anti-CTLA-4 and PD-1 [25]; (2) Emerging clinical evidence suggests that various ICD inducers commonly used in the anti-tumoral treatment can enhance effects of immunotherapy with ICBs, as long as they do not impair immunostimulatory signals or the activity of TILs [26]; (3) Immunosuppressive cells such as Treg cells, M2-polarized TAMs, and MDSCs are known to counteract ICD directly. Overall, these results suggest that FNC's diverse mechanisms result in synergistic effects with anti-PD-1 regimens. Furthermore, FNC has shown the capacity to stimulate an inflammatory response leading to the activation of CTL-driven adaptive immunity, thus facilitating the development of long-term immunological memory.

In our current study, another intriguing finding is that FNC demonstrates a potential synergistic anti-tumor effect when combined with anti-PD-1 therapy, leading to complete tumor regression in all treated immunocompetent tumor-bearing mice. This remarkable result suggests that FNC can enhance the efficacy of ICIs by mitigating immunosuppressive mechanisms within the TME and promoting a more favorable immune milieu for T cell activation and tumor clearance. The potential underlying mechanism for this synergy may involve the modulation of the TME by FNC, which includes enhancing the priming capacity of APCs, such as dendritic cells. Improved antigen presentation leads to more effective activation of T cells. Combined with ICIs, which block the immune inhibitory signals, results in a more robust and sustained anti-tumor immune response. This dual action of enhancing antigen presentation and relieving inhibitory signals within the TME provides a compelling rationale for using FNC and ICIs to achieve superior therapeutic outcomes in cancer treatment [27].

Our pathway enrichment analysis robustly implicates PD-1 signaling as a central transcriptional hub remodeled by FNC monotherapy. Across all analytical frameworks—GO, Reactome, and gene percentage metrics —PD-1 signaling emerged as the most significantly perturbed pathway (highest $-\log_{10}(P\text{-value}) \approx 12$; Rich factor > 0.4; ≈50% pathway gene representation). This consistent dominance suggests that FNC intrinsically targets the PD-1 axis, potentially reversing T cell exhaustion independently of anti-PD-1 co-treatment. While these transcriptomic data align with our observed synergy between FNC and anti-PD-1 therapy, they extend the mechanism by revealing FNC's capacity to autonomously rewire this immunosuppressive checkpoint at the transcriptional level. Notably, PD-1 signaling co-enriched with downstream TCR signaling and Immunoregulatory interactions, implying coordinated reinvigoration of T cell activation. Future studies should validate whether FNC directly suppresses PD-1 protein expression on TILs, a finding that would solidify its role as a novel immune checkpoint modulator.

In summary, our current studies demonstrate that the anti-tumor effects of FNC on various solid tumors primarily depend on the immune system. Concurrently, using single-cell multi-omics techniques, the existing results indicate that FNC' s anti-tumor effects are accompanied by substantial regulation of the immunosuppressive microenvironment. FNC reduces the infiltration of various immunosuppressive cells while increasing the exposure of DAMPs on the surface of tumor cells at the molecular and protein levels, promoting ICD-mediated programmed cell death. Lastly, by exploring the in vivo anti-tumor efficacy of FNC combined with immunotherapy in multiple solid tumors, we further confirmed the synergistic anti-tumor effects of FNC and anti-PD-1 antibodies. These findings provide solid evidence for the feasibility of FNC in anti-tumor therapy and its potential application in combination with existing anti-tumor therapies.

Acknowledgements

The research experiments delineated in this article were facilitated with the invaluable support of WuXi AppTec's Oncology and Immunology Unit (OIU). The authors thank the OIU team at WuXi AppTec for their indispensable technical support. Notably, our special acknowledgments extend to Qingyang Gu, Feifei Fan, Jingjing Wang, and Beibei Liu for their instrumental contributions to this project. Additionally, our gratefulness is expressed to the Crown Bioscience Inc. team and Frontage New-Drug, Inc. team for their supportive involvement, including team members Jin Cui, Demi Liu, Xuefei Yan, Yahong Zhang, Jianxin Yang, Dong Huang, Yuting Ji, Yimin Jiang, Dejun Wang, and Lianqi Zhao, Liu Shi.

Compliance with ethics guidelines

Conflicts of interest Limin Jia, Zhaoyang Wang, Jinfa Du, Zhigang Ren, Jiandong Jiang, and Pan Li declare that they have no conflicts of interest.

All institutional and national guidelines for the care and use of laboratory animals were followed.

Data availability and compliance statement

The authors declare that the acquisition and subsequent use of all data presented in this manuscript comply fully with all relevant local, national, and international laws, regulations, ethical guidelines, and the terms of use associated with the original data sources.

The authors bear full legal responsibility for ensuring the legality of data acquisition and all subsequent uses.

All data generated or analyzed during this study, which support the findings of this study, are available from the corresponding author on reasonable request. To request access to the data, please contact Dr. Pan Li.

Electronic supplementary material Supplementary material is available in the online version of this article at https://doi.org/10.1007/s11684-025-1164-0 and is accessible for authorized users

References

1. Groth C, Hu X, Weber R, Fleming V, Altevogt P, Utikal J, Umansky V. Immunosuppression mediated by myeloid-derived suppressor cells (MDSCs) during tumour progression. Br J Cancer 2019; 120(1): 16–25
2. Umansky V, Sevko A. Tumor microenvironment and myeloid-derived suppressor cells. Cancer Microenviron 2013; 6(2): 169–177
3. Zou Z, Lin H, Li M, Lin B. Tumor-associated macrophage polarization in the inflammatory tumor microenvironment. Front Oncol 2023; 13: 1103149
4. Huang A, Cao S, Tang L. The tumor microenvironment and inflammatory breast cancer. J Cancer 2017; 8(10): 1884–1891
5. Dong P, Yan Y, Fan Y, Wang H, Wu D, Yang L, Zhang J, Yin X, Lv Y, Zhang J, Hou Y, Liu F, Yu X. The role of myeloid-derived suppressor cells in the treatment of pancreatic cancer. Technol Cancer Res Treat 2022; 21: 15330338221142472
6. Joshi S, Sharabi A. Targeting myeloid-derived suppressor cells to enhance natural killer cell-based immunotherapy. Pharmacol Ther 2022; 235: 108114
7. Wang JC, Sun L. PD-1/PD-L1, MDSC pathways, and checkpoint inhibitor therapy in Ph(-) myeloproliferative neoplasm: a review. Int J Mol Sci 2022; 23(10): 5837
8. Anderson HG, Takacs GP, Harris DC, Kuang Y, Harrison JK, Stepien TL. Global stability and parameter analysis reinforce therapeutic targets of PD-L1-PD-1 and MDSCs for glioblastoma. J Math Biol 2023; 88(1): 10
9. Fayzullina D, Kharwar RK, Acharya A, Buzdin A, Borisov N, Timashev P, Ulasov I, Kapomba B. FNC: an advanced anticancer therapeutic or just an underdog? Front Oncol 2022; 12: 820647
10. Zhao L, Li S, Zhong W. Mechanism of action of small-molecule agents in ongoing clinical trials for SARS-CoV-2: a review. Front Pharmacol 2022; 13: 840639
11. Zhang Y, Zhang R, Ding X, Peng B, Wang N, Ma F, Peng Y, Wang Q, Chang J. FNC efficiently inhibits mantle cell lymphoma growth. PLoS One 2017; 12(3): e0174112
12. Amiri M, Molavi O, Sabetkam S, Jafari S, Montazersaheb S. Stimulators of immunogenic cell death for cancer therapy: focusing on natural compounds. Cancer Cell Int 2023; 23(1): 200
13. Zhang JL, Li YH, Wang LL, Liu HQ, Lu SY, Liu Y, Li K, Liu B, Li SY, Shao FM, Wang K, Sheng N, Li R, Cui JJ, Sun PC, Ma CX, Zhu B, Wang Z, Wan YH, Yu SS, Che Y, Wang CY, Wang C, Zhang Q, Zhao LM, Peng XZ, Cheng Z, Chang JB, Jiang JD. Azvudine is a thymus-homing anti-SARS-CoV-2 drug effective in treating COVID-19 patients. Signal Transduct Target Ther 2021; 6(1): 414
14. de Souza SB, Cabral PGA, da Silva RM, Arruda RF, Cabral SPF, de Assis A, Viana AB Junior, Degrave WMS, Moreira ADS, Silva CG, Chang J, Lei P. Phase III, randomized, double-blind, placebo-controlled clinical study: a study on the safety and clinical efficacy of AZVUDINE in moderate COVID-19 patients. Front Med (Lausanne) 2023; 10: 1215916
15. Zhu KW. Efficacy and safety evaluation of Azvudine in the prospective treatment of COVID-19 based on four phase III clinical trials. Front Pharmacol 2023; 14: 1228548
16. Qi X, Yang Y, Gong B, Li Z, Liang D. Real-world effectiveness of azvudine for patients infected with the SARS-CoV-2 omicron subvariant BA. 5 in an intensive care unit. J Thorac Dis 2023; 15(9): 4925–4937
17. Sun L, Peng Y, Yu W, Zhang Y, Liang L, Song C, Hou J, Qiao Y, Wang Q, Chen J, Wu M, Zhang D, Li E, Han Z, Zhao Q, Jin X, Zhang B, Huang Z, Chai J, Wang JH, Chang J. Mechanistic insight into antiretroviral potency of 2′-deoxy-2′-beta-fluoro-4′-azidocytidine (FNC) with a long-lasting effect on HIV-1 prevention. J Med Chem 2020; 63(15): 8554–8566
18. Wu Y, Yi M, Niu M, Mei Q, Wu K. Myeloid-derived suppressor cells: an emerging target for anticancer immunotherapy. Mol Cancer 2022; 21(1): 184

19. Ge Y, Cheng D, Jia Q, Xiong H, Zhang J. Mechanisms underlying the role of myeloid-derived suppressor cells in clinical diseases: good or bad. Immune Netw 2021; 21(3): e21
20. Chen DS, Mellman I. Elements of cancer immunity and the cancer-immune set point. Nature 2017; 541(7637): 321–330
21. Sharma P, Hu-Lieskovan S, Wargo JA, Ribas A. Primary, adaptive, and acquired resistance to cancer immunotherapy. Cell 2017; 168(4): 707–723
22. Cai Z, Guo H, Qian J, Liu W, Li Y, Yuan L, Zhou Y, Lin R, Xie X, Yang Q, Wu G, Li Q, Zhao L, Liu F, Wang J, Lu W. Effects of bone morphogenetic protein 4 on TGF-β1-induced cell proliferation, apoptosis, activation and differentiation in mouse lung fibroblasts via ERK/p38 MAPK signaling pathway. PeerJ 2022; 10: e13775
23. Ding M, Zhang Y, Yu N, Zhou J, Zhu L, Wang X, Li J. Augmenting immunogenic cell death and alleviating myeloid-derived suppressor cells by sono-activatable semiconducting polymer nanopartners for immunotherapy. Adv Mater 2023; 35(33): 2302508
24. Alghamri MS, Banerjee K, Mujeeb AA, Mauser A, Taher A, Thalla R, McClellan BL, Varela ML, Stamatovic SM, Martinez-Revollar G, Andjelkovic AV, Gregory JV, Kadiyala P, Calinescu A, Jimenez JA, Apfelbaum AA, Lawlor ER, Carney S, Comba A, Faisal SM, Barissi M, Edwards MB, Appelman H, Sun Y, Gan J, Ackermann R, Schwendeman A, Candolfi M, Olin MR, Lahann J, Lowenstein PR, Castro MG. Systemic delivery of an adjuvant CXCR4-CXCL12 signaling inhibitor encapsulated in synthetic protein nanoparticles for glioma immunotherapy. ACS Nano 2022; 16(6): 8729–8750
25. De Cicco P, Ercolano G, Ianaro A. The new era of cancer immunotherapy: targeting myeloid-derived suppressor cells to overcome immune evasion. Front Immunol 2020; 11: 1680
26. Pfirschke C, Engblom C, Rickelt S, Cortez-Retamozo V, Garris C, Pucci F, Yamazaki T, Poirier-Colame V, Newton A, Redouane Y, Lin YJ, Wojtkiewicz G, Iwamoto Y, Mino-Kenudson M, Huynh TG, Hynes RO, Freeman GJ, Kroemer G, Zitvogel L, Weissleder R, Pittet MJ. Immunogenic chemotherapy sensitizes tumors to checkpoint blockade therapy. Immunity 2016; 44(2): 343–354
27. Yi M, Zheng X, Niu M, Zhu S, Ge H, Wu K. Combination strategies with PD-1/PD-L1 blockade: current advances and future directions. Mol Cancer 2022; 21(1): 28